Materials Research. 2020; 23(2): e20200083
DOI: https://doi.org/10.1590/1980-5373-MR-2020-0083

Isolating the Effects of Mg^{2+}, Mn^{2+} and Sr^{2+} Ions on Osteoblast Behavior from those Caused by Hydroxyapatite Transformation

Leila Melo da Silva[a], Débora dos Santos Tavares[b], Euler Araujo dos Santos[a,c]*

[a]*Universidade Federal de Sergipe, Programa de Pós-Graduação em Ciência e Engenharia de Materiais (P²CEM), Av. Marechal Rondon, s/n, 49100-000, São Cristóvão, SE, Brasil*
[b]*Universidade Federal de Sergipe, Departmento de Educação em Saúde, Av. Governador Marcelo Déda, 13, 49400-000, Lagarto, SE, Brasil*
[c]*Universidade Federal do Sergipe, Departmento de Ciência e Engenharia de Materiais, Av. Marechal Rondon, s/n, 49100-000, São Cristóvão, SE, Brasil*

Received: February 27, 2020; Revised: March 25, 2020; Accepted: April 7, 2020

Ionic trace elements such as Mg^{2+}, Mn^{2+} and Sr^{2+} are very difficult to stabilize in the hydroxyapatite lattice, and they can induce phase transformations when subjected to thermal treatments. The effects of the ions themselves are often confused with the effects of the newly formed phases. Therefore, the objective of this work was to evaluate the effects of the ions isolated from the effects caused by the inherent phase transformations observed in these systems. WDXRF, XRD, FTIR and biological assays using mouse preosteoblastic cells (MC3T3-E1) showed the Mg^{2+} ions can stimulate cell differentiation even when segregated from the HA structure in the form of MgO. However, the presence of MgO considerably retards cell proliferation. At the same time, Mn^{2+} ions are able to increase cell proliferation and induce the production of high levels of ALP, regardless of whether they are inserted into the HA structure or segregated in the form of Mn_3O_4. Finally, the presence of Sr^{2+} in the HA lattice does not appear to directly affect cell behavior, since both the proliferation and production of ALP are comparable to those observed in the nondoped HA sample.

Keywords: *hydroxyapatite, trace element, osteoblast behavior, MC3T3-E1, phase transformation.*

1. Introduction

The insertion of trace elements into the hydroxyapatite structure $[Ca_{10}(PO_4)_6(OH)_2]$ is widely proposed as an important way to improve the biocompatibility of bone grafts and implants used in the treatment of bone diseases[1-3]. Its structure can accommodate doping ions of different sizes and charges, either individually or simultaneously[4-6]. The family of apatite minerals have the general formula $M_{10}(XO_4)_6(Y)_2$, where M refers to mono-, di- or trivalent ions, such as Ag^+, Na^+, Ca^{2+}, Sr^{2+}, Mg^{2+}, Mn^{2+} and Zn^{2+}; XO refers to PO_4^{3-}, CO_3^{2-}, HPO_4^{2-} or SO_4^{2-}; and Y refers to OH^-, CO_3^{2-}, Cl^- or F^-[6-8]. Apatite minerals can be found in nature from metamorphic transformations in the Earth's crust[9-11] or from biomineralized deposits in living organisms[12-14]. The biomineralized hydroxyapatite found in bone tissue is also highly substituted with trace elements, making it a large reservoir of ionic nutrients necessary for life[5,12].

Being multisubstituted, biomineralized hydroxyapatite is very different from typical hydroxyapatites synthesized in the laboratories, and it is easier to evaluate the effect of one element on the cells if this element is the only dopant in the structure. For this reason, the isolated effects of trace elements on cells, specifically cells in bone tissue, have been continuously studied. Mg^{2+} influences bone metabolism, stimulating osteoblast proliferation, especially at the beginning of osteogenesis[2,15,16]. Mn^{2+} is involved in the regulation of bone remodeling and activates integrins, improving cellular adhesion[5,17,18]. Sr^{2+} exhibits beneficial effects on bone formation and resorption processes through osteoblast stimulation and inhibition of osteoclast activity[2,19-21]. However, these effects are often attributed to one specific element without accounting for the contributions of the phase transformations that occur in the studied system. The presence of trace elements in hydroxyapatites can produce small phase transformations during thermal treatments, which are required due to the difficulty of introducing these elements into the apatitic lattice[15,22-27]. Therefore, in many cases, the effects attributed to one element in the doped hydroxyapatites are mixed with those caused by the presence of phases that are unaccounted for. For instance, Webler et al.[28] observed that the level of Mg^{2+} and the concentration of phases in biphasic ceramics (β-TCP/hydroxyapatite) had no effect on macrophage viability after 24 h of culture. In this case, two factors were simultaneously influencing this system: Mg^{2+} and the β-TCP/hydroxyapatite concentration. Bhattacharjee et al.[29] attributed the differences observed in the in vivo behavior of hydroxyapatite implants to the presence of Zn^{2+} but did not consider the presence of the β-TCP phase generated when these implants were calcined at 800 and 1150°C. Likewise, Ullah et al.[30] studied the role of Fe/Sr-doped dielectric hydroxyapatites on the adhesion and proliferation of human mesenchymal stem cells (hMSCs). The singular Fe-substituted group showed better cell proliferation than the singular Sr-substituted

*e-mail: euler@ufs.br

group and the pristine group. This difference was attributed to the biological role of the Fe and Sr ions released from the ceramic over time. However, the insertion of Fe and/or Sr into hydroxyapatite induced a phase transformation at 1100°C, yielding a multiphasic ceramic with at least 52% β-TCP and different amounts of Fe_2O_3. Again, the effect of the dopant itself was overlaid with the effect of the presence of different phases in the sample. Therefore, many of the effects attributed to one specific element in the doped hydroxyapatites on cellular behavior or in vivo performance are not adequately explained.

Recently, we studied mechanisms by which it is possible to stabilize several cations in a multisubstituted hydroxyapatite[31]. We verified that some ions that are more difficult to insert into the hydroxyapatite lattice can be more easily incorporated if they are in the presence of other cations or counterions such as carbonate[31,32]. Using the Rietveld refinement on the X-ray diffraction data, the insertion of the ions into the hydroxyapatite phase or their segregation in other phases during calcination could be confirmed. Therefore, our objective in this work was to start from similar systems comprising Mg^{2+}-, Mn^{2+}- and Sr^{2+}-doped hydroxyapatite to isolate the effects on osteoblast behavior caused by the doping element itself from those caused by the presence of other phases formed during the heat treatment.

2. Materials and Methods

2.1. HA synthesis

2.1.1. Pure HA

The pure HA powder was obtained by a aqueous precipitation method through a reaction between phosphoric acid (0.220 mol L^{-1}) and calcium hydroxide (0.334 mol L^{-1}). The reaction was conducted at 60°C under stirring, and the pH was maintained at 10 with the addition of sodium hydroxide. After 24 h of aging, the precipitate was filtered, washed with distilled water, dried at 120°C for 24 h, and sieved (106 μm).

2.1.2. Doped HA

The same procedure described above was employed to synthesize the doped HA samples. Sr^{2+}, Mg^{2+} and Mn^{2+} ions were added to the reaction medium as follows: magnesium and strontium chloride were dissolved in the calcium hydroxide suspension, while manganese chloride was dissolved in the phosphoric acid solution to avoid Mn^{2+} oxidation. The relative ratio between the doping ions and Ca^{2+}, *i.e.*, $M^{2+}/(Ca^{2+} + M^{2+})$, was kept at 0.04 (4 mol %). The reagents were purchased from Sigma-Aldrich and had a purity above 99%.

2.2. Powder processing

The thermal stability of the samples was studied after calcining the obtained powders for 2 h at 1000°C under a heating rate of 2.8°C/min. For the cell culture assays, pellets 10 mm in diameter and 1.0 mm in height were made by uniaxial pressing of the prepared HA powders under a load of 237 MPa. After pressing, the obtained tablets were calcined under the conditions described above for the powders.

2.3. Physicochemical characterization

2.3.1. Elemental composition

The elements in the samples were identified and quantified by wavelength-dispersive X-ray fluorescence spectroscopy (WDXRF) using a Bruker S8-Tiger 4 kW spectrometer equipped with LiF 200, PET, XS-5 and XS-C crystals. The calcined powders were pressed into pellets and directly analyzed. A calibration curve was established using a standard hydroxyapatite (Ca/P = 1.67) powder mixed in 6 different proportions with standard strontium, manganese and magnesium nitrate powders. The mixtures were homogenously ground in a ball mill apparatus for 30 min at 350 rpm, and a curve was constructed by analyzing each mixture in tablet form. All reagents were of high purity (≥ 99.5%) and were purchased from Sigma-Aldrich.

2.3.2. Structural changes

The structural changes were studied by X-ray diffraction (XRD) using a Shimadzu XRD 6000 diffractometer (CuKα λ = 1.5405 Å; 60 kV, 55 mA, Ni filter, scintillation detector). The samples were scanned from 10º to 60º with a step size of 0.02º and an acquisition time of 2 s per point. The diffraction patterns were refined using the Rietveld method (HighSchore Plus), which allowed us to follow the phase transformations and lattice parameter changes in the hydroxyapatite phase.

2.3.3. Molecular groups in the HA phase

The changes in the functional groups in the HA phase, such as PO_4^{3-} and OH^-, were observed by Fourier transform infrared (FTIR) spectroscopy on a Perkin-Elmer 1720X apparatus. The insertion of HPO_4^{2-}, CO_3^{2-} and other species was investigated. The spectra were acquired in the range of 4000 to 400 cm^{-1} with a resolution of 1 cm^{-1}. The samples were prepared by mixing with anhydrous KBr and pressing into pellets.

2.4. Biological assays

2.4.1. Osteoblast culture

Mouse preosteoblastic cells (MC3T3-E1) were cultured in 75-cm^2 flasks containing alpha-MEM culture medium (Sigma) supplemented with 10% fetal bovine serum (FBS) and antibiotics (100 U/mL penicillin and 100 μg/mL streptomycin) in an incubator at 37ºC under a humidified atmosphere of 95% air and 5% CO_2. After reaching confluence, the cells were trypsinized, resuspended in complete medium and counted in a Neubauer chamber. The ceramic samples were sterilized by heating in air at 180ºC for 2 h. Sterilization by autoclaving was avoided because of the possible induction of surface phase transformations and dissolution. The samples were placed into a culture plate and immersed for 1 h in 1000 μL of alpha-MEM culture medium (Sigma-Aldrich) supplemented with 10% FBS and antibiotics. Then, the medium was discarded, and 15 μL of cell suspension containing 1.0×10^4 cells was seeded on each sample, and the samples were left for 1 h in an incubator to allow cell adhesion onto the sample instead of the bottom of the well. The wells were then filled with 1000 μL of the culture medium

supplemented with antibiotics. The cells were monitored after 7, 14 and 21 days of culture.

2.4.2. Cellular growth: MTT assay

At each time point, the samples were gently rinsed with PBS solution to remove nonadherent cells. Five hundred microliters of 5 mg/mL MTT [3-(4,5-dimethylthiazol-2-yl)-2,5-diphenyl tetrazolium bromide] solution (Sigma-Aldrich) was added to the remaining cells, and they were incubated for 3 h at 37°C under a humidified atmosphere of 95% air and 5% CO_2. Viable cells convert the yellow tetrazolium salt (MTT) into blue formazan crystals. Afterwards, the MTT was removed, and the cells were immersed in 500 µL of acidic isopropanol to dissolve the intracellular formazan crystals produced by live cells. The absorbance was determined at 570 nm using an ELISA reader. The cell number was obtained based on the linear correlation between the absorbance and the MC3T3-E1 cell concentration (from 1×10^4 to 5×10^4 cells/mL). The cell number was adjusted to the surface area of the sample and is expressed in cells/mm^2. The experiment was conducted in triplicate.

2.4.3. Cellular differentiation: ALP activity

Alkaline phosphatase (ALP) activity was assessed by examining the hydrolysis of *p*-nitrophenyl phosphate (Sigma-Aldrich) in an alkaline buffer solution (substrate). At each time point, the cells plated on the surfaces were permeabilized in 0.5% Triton X-100 (octylphenol ethoxylate) (Sigma-Aldrich) in water and incubated for 30 min with the substrate. The reaction was ended by the addition of 0.1 mol L^{-1} EDTA in a 1 mol L^{-1} NaOH solution. Colorimetric determination of the product (p-nitrophenol) was carried out at 405 nm (ELISA reader). ALP activity was calculated from a standard curve (from 50 up to 3200 nmol *p*-nitrophenyl phosphate/L), and the results were expressed in nanomols (nmol) of *p*-nitrophenol produced per 10^4 cells.

2.5. Statistical analyses

All values are expressed as the mean ± standard deviation. The statistical significance of the obtained data was assessed using one-way ANOVA followed by Tukey's test. Differences at $p \geq 0.05$ were considered not statistically significant.

3. Results and Discussion

In a previous work[31], we demonstrated that the amounts of Sr^{2+}, Mg^{2+} and Mn^{2+} ions present in the precipitated hydroxyapatite phase were not similar. Since their concentrations in the reaction medium were not equal, it was not possible to precisely evaluate the competition among the elements for sites in the hydroxyapatite lattice or their isolated effects on the physicochemical and biological properties. In addition, two different counterions were used during the synthesis (chloride and nitrate), making the obtained results more complex, as discussed in another work[32]. Therefore, in the present work, we made significant changes to the methodology to specifically evaluate the isolated effects of each element on the physicochemical and biological properties, as follows: a) the relative ratio between the doping ions and Ca^{2+}, *i.e.*, $M^{2+}/(Ca^{2+}+M^{2+})$ was kept at 0.04 (4 mol %) for all conditions and b) only chloride was used as a counterion. After making these changes, we considerably reduced the number of variables, making it possible to isolate the effects of each element on the hydroxyapatite properties.

3.1. Effect of the doping elements on the hydroxyapatite structure

The results obtained by WDXRF demonstrated that the presence of one element did not affect the capture of others during the precipitation process. The amount of Mg present in the samples was not significantly influenced by the presence of Sr or Mn (Figure 1a). Similarly, the amount of Mn was not influenced by the presence of Mg or Sr (Figure 1b), and the amount of Sr was not influenced by the presence of Mg or Mn (Figure 1c). However, the amount of Sr was always lower than the measured amounts of Mg and Mn. This means that, in competitive terms, the capture of Sr^{2+} during the precipitation process was less favorable than the capture of Mg^{2+} and Mn^{2+} when they were present at the same concentration in the reaction medium.

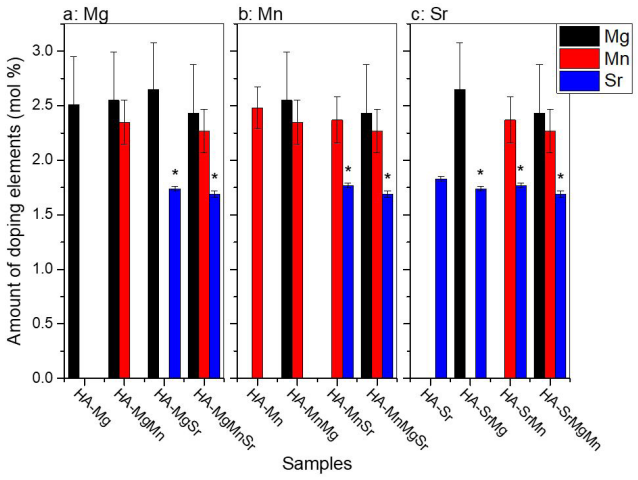

Figure 1. Amount of each dopant in the samples as measured by WDXRF. The effect of Mn^{2+} and Sr^{2+} on the amount of Mg^{2+} (a), the effect of Mg^{2+} and Sr^{2+} on the amount of Mn^{2+} (b), and the effect of Mg^{2+} and Mn^{2+} on the amount of Sr^{2+} (c). *Significantly different from the amount of the element in the initial mixture: Mg^{2+} (a), Mn^{2+} (b) and Sr^{2+} (c).

The Gibbs free energies of hydration ($\Delta_{hyd}G°$/kJ mol^{-1}) for Sr^{2+}, Ca^{2+}, Mn^{2+} and Mg^{2+} ions are 1380, 1505, 1760 and 1830, respectively[33]. In general, the higher the energy of hydration is, the stronger the interaction between the ion and water molecules in the solvation shell[34]. This strong interaction hinders further interactions between the ion and interfaces, for instance, in an adsorption process. Thus, it was expected that the capture of Mn^{2+} and Mg^{2+} by the hydroxyapatite clusters during nucleation and growth would be less pronounced than that observed for Sr^{2+} ions. In this case, the energy of hydration should not be the most important factor influencing the accommodation of these ions in the HA structure. In fact, the HA structure presents two Ca^{2+} sites (Ca[I] and Ca[II]) with different chemical environments that accommodate ions in different ways. Therefore, the affinity of these ions for each site must be the dominant factor controlling the amount of ions incorporated into the structure.

Precipitation occurred without atmospheric control, and under such conditions, CO_2 can be dissolved in the reaction medium, resulting in CO_3^{2-} ions[35]. This means that, in addition to the doping elements (Mg^{2+}, Sr^{2+} and Mn^{2+}), CO_3^{2-} ions were also available to be captured during the precipitation process. The presence of CO_3^{2-} in the obtained sample was monitored by FTIR spectroscopy. The relative intensity changes in the ν_2 CO_3^{2-} and ν_4 PO_4^{3-} absorption bands made it possible to estimate the relative levels of CO_3^{2-} captured by the precipitates. The results demonstrated that the presence of the doping elements affected the capture of CO_3^{2-}. In general, the presence of Mg^{2+}, Sr^{2+} and Mn^{2+} inhibited the capture of CO_3^{2-} ions (Figure 2), which was verified by the remarkable decreases in the ν_2 CO_3^{2-}/ν_4 PO_4^{3-} intensity ratios observed in the spectra of the as-synthesized samples. The calcination process decreases these intensity ratios even more, meaning that CO_3^{2-} groups were released during the thermal treatment

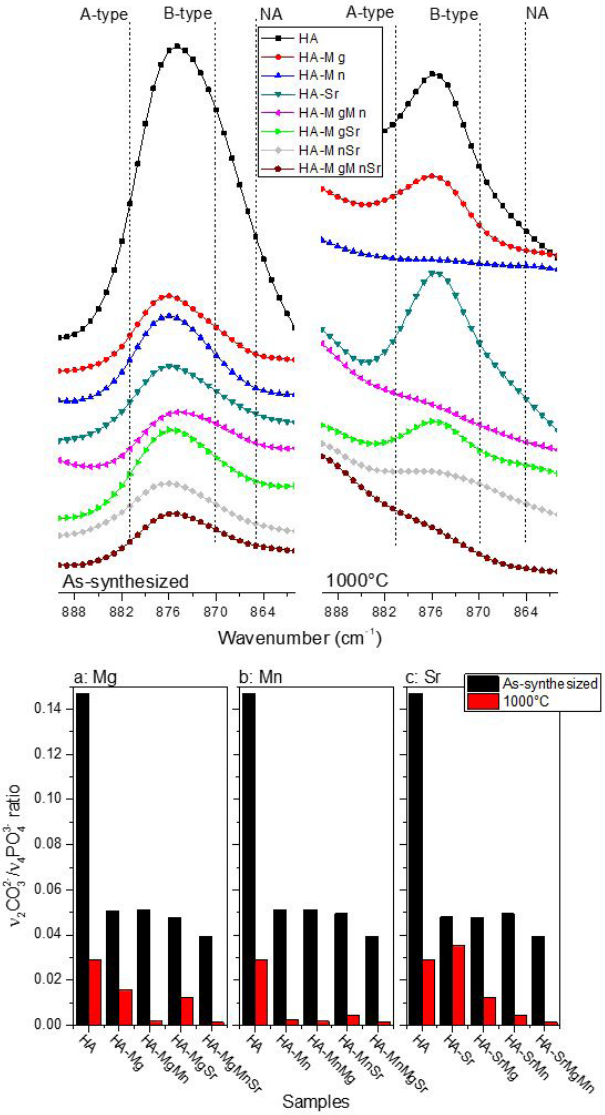

Figure 2. FTIR spectra and intensity ratios for the ν_2 CO_3^{2-} and ν_4 PO_4^{3-} absorption bands before and after calcination at 1000°C. The effect of Mn^{2+} and Sr^{2+} on Mg^{2+} (a), the effect of Mg^{2+} and Sr^{2+} on Mn^{2+} (b), and the effect of Mg^{2+} and Mn^{2+} on Sr^{2+} (c).

in the form of CO_2[31,32,36]. This release was more pronounced for the Mn^{2+}-containing samples and less pronounced for the pure and Sr^{2+}-containing samples. The inherent inclusion of CO_3^{2-} into the apatite lattices during precipitation is very well known and has also been observed in biomineralization processes[35,37]. In several cases, the simultaneous inclusion of this ion along with other doping elements into an apatite lattice can thermally stabilize the structure[31,32,38,39].

The (Ca+M)/P ratios measured for all samples were always above 1.67 (Table 1), indicating the formation of nonstoichiometric hydroxyapatites. (Ca+M)/P ratios above 1.67 could mean either an excess of cations or insufficient phosphate groups[13,40]. As observed by FTIR spectroscopy (Figure 2), the sample obtained in the absence of a dopant (HA) exhibited the highest $\nu_2\ CO_3^{2-}/\nu_4\ PO_4^{3-}$ ratio, with an evident B-type substitution (replacement of the PO_4^{3-} groups with CO_3^{2-})[41]. Therefore, the high (Ca+M)/P ratio measured for the HA sample was likely caused by the insertion of CO_3^{2-} into the PO_4^{3-} sites. As mentioned before, the $\nu_2\ CO_3^{2-}/\nu_4\ PO_4^{3-}$ ratio was significantly lower for the samples prepared in the presence of the dopants. In these cases, the high values observed for the (Ca+M)/P ratios could mean the effective insertion of cations into the hydroxyapatite structure, especially if one considers that no phases other than hydroxyapatite were present in the as-synthesized samples, as demonstrated by the XRD analyses (Figure 3a). The presence of the doping elements did not induce the precipitation of phases other than hydroxyapatite. However, a high (Ca+M)/P ratio for the hydroxyapatite structure means that the excess cations are likely segregated in the form of oxides during the thermal treatments. Indeed, after calcination at 1000°C, the hydroxyapatite phase became more crystalline (Figure 3b), and small phase transformations were observed, which were appropriately quantified by Rietveld refinement.

The HA sample was altered by thermal treatment, producing 5.3 wt. % calcium oxide (CaO) (Figure 4). The insertion of Mg^{2+} reduced the CaO formation to 0.3 wt. % but induced the appearance of 1.8 wt. % magnesium oxide (MgO). This indicates the segregation of approximately 2.7 mol % of Mg^{2+} from the as-synthesized hydroxyapatite phase. Considering the standard deviation observed in the WDXRF results (Figure 1), one can conclude that all the Mg^{2+} ions were segregated from the apatite phase, having been transformed into MgO after calcination.

The effect of the simultaneous insertion of Mg^{2+} and Sr^{2+} did not appear to be different from the effect of Mg^{2+} alone (Figure 4a). However, the simultaneous insertion of Mg^{2+} and Mn^{2+} inhibited the formation of CaO and MgO and resulted in the appearance of 3.6 wt. % Mn_3O_4. If we take into account the 2.3 mol % Mn^{2+} measured in the HA-MgMn sample and the error associated with the WDXRF analysis, it is possible to say that all Mn^{2+} ions were segregated from the apatite phase after calcination. The same behavior was observed for the simultaneous insertion of the three elements (Figure 4a), indicating that Sr^{2+} had a negligible effect on this phase transformation. On the other hand, the insertion of Mn^{2+} alone (Figure 4b) completely inhibited the formation of CaO relative to that seen in pure HA, and Mn_3O_4 was also not formed.

The small influence of Sr^{2+} on these phase transformations was confirmed by the fact that the insertion of this ion alone reduced the formation of CaO from 5.3 wt. % (HA sample) to 2.0 wt. % but the transformations previously attributed to the Mg^{2+} and Mn^{2+} ions were unchanged (Figure 4c). In fact, the formation of strontium oxide (SrO) was not observed, suggesting that the Sr^{2+} ions are adequately stabilized in the apatite structure, regardless of the insertion of the other ions.

To confirm whether the doping elements were inserted into the apatite lattice or were completely segregated, as suggested in the previous discussion, we analyzed the changes in the hydroxyapatite unit cell volume before and after calcination for all conditions (Figure 5). Because it is smaller than Ca^{2+} (1.00 Å)[13,33], Mg^{2+} (0.72 Å) should induce a decrease in the unit cell volume. However, no significant changes were observed for the HA-Mg sample compared to the HA sample (Figure 5a). This behavior can be evaluated

Table 1. Ca/P and (Ca+M)/P ratios obtained from WDXRF. M = Mg, Sr and/or Mn.

Samples	Ca/P	(Ca+M)/P
HA	1.74	1.74
HA-Mg	1.68	1.75
HA-Sr	1.66	1.71
HA-Mn	1.65	1.72
HA-MgSr	1.63	1.74
HA-MgMn	1.65	1.78
HA-SrMn	1.63	1.74
HA-MgSrMn	1.60	1.77

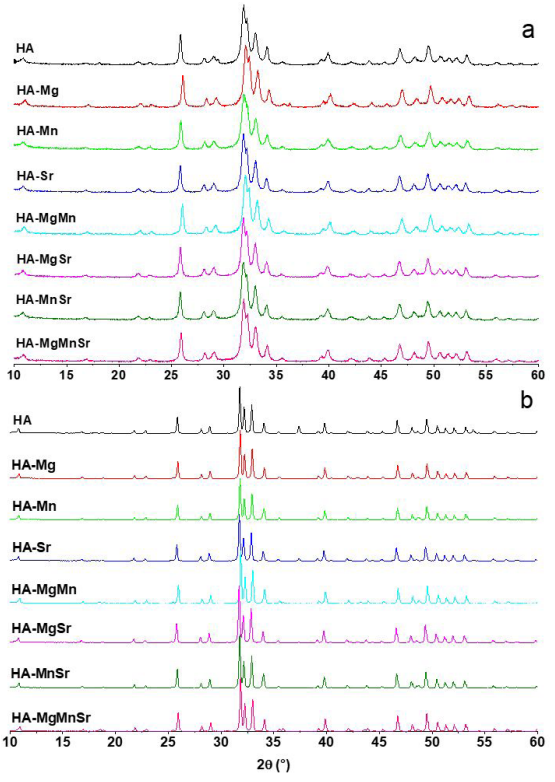

Figure 3. XRD patterns of the a) as-synthesized samples and b) samples after calcination at 1000°C.

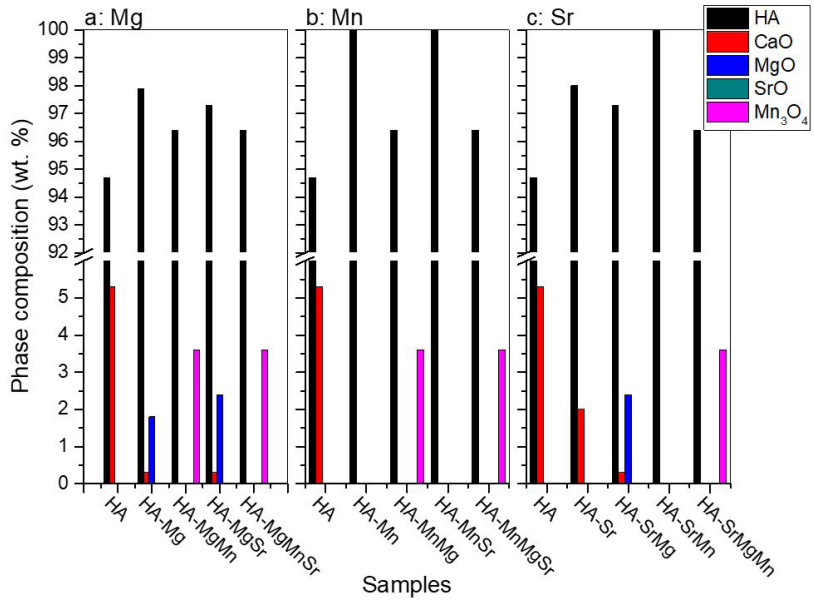

Figure 4. Phase composition of each sample after calcination at 1000°C as a function of the doping elements. The effect of Mn^{2+} and Sr^{2+} on Mg^{2+} (a), the effect of Mg^{2+} and Sr^{2+} on Mn^{2+} (b), and the effect of Mg^{2+} and Mn^{2+} on Sr^{2+} (c).

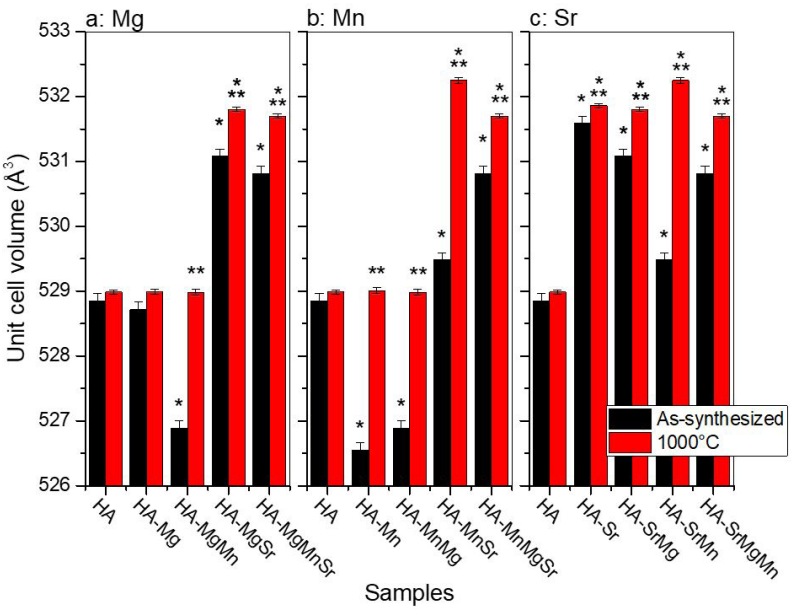

Figure 5. Unit cell volume calculated from the HA phase before and after calcination at 1000°C as a function of the doping elements. The effect of Mn^{2+} and Sr^{2+} on Mg^{2+} (a), the effect of Mg^{2+} and Sr^{2+} on Mn^{2+} (b), and the effect of Mg^{2+} and Mn^{2+} on Sr^{2+} (c). *Significantly different from the HA samples. **Significant difference between the as-synthesized and calcined samples in the same group.

by comparing the samples before and after calcination. Before calcination, one can suppose that the unit cell volume measured for the HA-Mg sample already included the volume contraction caused by the insertion of the Mg^{2+} ions into the hydroxyapatite lattice. Similarly, the insertion of CO_3^{2-} ions into the apatite lattice is also known to decrease the unit cell volume[42,43]. If one considers that the amount of CO_3^{2-} inserted in the HA sample was considerably higher than that inserted in the HA-Mg sample, one can conclude that the volume contraction induced by the Mg^{2+} insertion in the HA-Mg sample was comparable to the contraction induced by the CO_3^{2-} insertion in the HA sample. This seems to be confirmed because after calcination, the volume remained the same for both the HA and HA-Mg samples. That is, after the release of the Mg^{2+} and CO_3^{2-} ions, the hydroxyapatite

phase had a composition closer to its standard stoichiometry in both the HA and HA-Mg samples.

The incorporation of Mn^{2+} ions tended to decrease the unit cell volume (Figure 5b). As discussed before, the insertion of Mn^{2+} alone or with Sr^{2+} ions was favorable when no phase transformation was observed. However, with associated with Mg^{2+}, the Mn^{2+} ions were completely segregated as Mn_3O_4 after calcination. For this reason, the volume contraction caused by the insertion of Mn^{2+} ions into the HA lattice was clearly observed.

In contrast to Mg^{2+}, Sr^{2+} ions significantly increased the unit cell volume of the hydroxyapatite phase (Figure 5c). Because it is larger than Ca^{2+}, Sr^{2+} (1.28 Å) tends to increase the unit cell volume[44]. When Sr^{2+} is no longer segregated during the calcination process in the form of SrO or other Sr-rich phases (Figure 4), its presence in the lattice did not cause any volume increase even after calcination. Therefore, it is possible to say that all the Sr^{2+} ions inserted into the samples are included in the hydroxyapatite phase.

3.2. Biological behavior

To isolate the effect of each element on cellular behavior, only the samples containing Mg^{2+}, Mn^{2+} or Sr^{2+} ions alone and the samples containing all three ions were compared with the nondoped HA sample.

After 7 days of culture, all the samples had essentially the same number of cells, except for the HA-Mg sample, which had a lower number of cells (Figure 6). This indicates that up to 7 days, the HA-Mg sample did not favor proliferation. However, at 14 days of culture, the number of cells significantly increased for all the samples. The proliferation profiles showed that the cells grew almost linearly over time. Thus, the cell growth rate for each sample could be calculated by deriving the number of cells as a function of time. The results showed that the highest proliferation rate occurred on the Mn^{2+}-containing samples (HA-Mn and HA-MgMnSr). The HA-Mn sample had the highest proliferation rate among all the samples (91 ± 26 cells mm^{-1} day^{-1}), followed by the HA-MgMnSr sample (76 ± 2 cells mm^{-1} day^{-1}). The lowest rate was observed on the HA sample (10 ± 2 cells mm^{-1} day^{-1}). Although the HA-Mg sample had the lowest number of cells after 7 days of culture, the proliferation rate was even higher than that of the cells on HA until the end of 21 days (36 ± 2 cells mm^{-1} day^{-1}). According to the phase composition data (Figure 4), all the Mn^{2+} ions in the HA-Mn sample were inserted into the apatite, but in the HA-MgMnSr sample, they were segregated as Mn_3O_4; nevertheless, the insertion of Sr^{2+} and Mg^{2+} was confirmed. One can assume that manganese plays a more significant role in cell proliferation, probably due to its vital role in the binding of integrins to ligands, which is the same process by which cells bind to substrates[45], stimulating osteoblast activity[46]. Huang et al.[47] cultivated MC3T3-E1 cells onto titanium discs coated with Mn^{2+}-doped hydroxyapatite and demonstrated a higher proliferation rate compared to cells on a pure hydroxyapatite coating after 7 days, corroborating our findings.

The beneficial effects of individual dopants in the apatite structure seem different when this element is associated with other elements. Inhibitory and stimulatory effects on cellular activity can be produced from this combination of factors[48,49]. These changes in activity are caused by physicochemical changes in the calcium phosphate samples, such as phase transformation and changes in crystallinity and solubility, which are induced by the presence of the ions[48]. Therefore, the effect of a dopant competes with other factors rather than being the only factor influencing cellular behavior. For this reason, our results need to be interpreted as a function of the phase composition observed for each sample after calcination. According to the results presented in Figure 4, several samples showed a small amount of oxide in their composition. Unlike Mn_3O_4, CaO and MgO are highly reactive with water, generating $Ca(OH)_2$ and $Mg(OH)_2$ as products, respectively. The solubility of the products, $Ca(OH)_2$ (pK_{sp} = 5.18) and $Mg(OH)_2$ (pK_{sp} = 11.14), at 25°C is much lower than that of Mn_3O_4 (pK_{sp} = 54.15), indicating that $Ca(OH)_2$ and $Mg(OH)_2$ can be readily dissolved in aqueous environments after formation.

It is possible to observe a close correlation between the cell proliferation rate and the presence of CaO and MgO in the samples. The samples that did not present these oxides showed higher proliferation rates (Figure 6). Therefore, one can assume that the oxide reaction would cause a local pH increase, significantly diminishing cellular proliferation. However, it is important to note that all the samples were immersed in supplemented medium for 1 h prior to seeding the cells. This medium was replaced with new medium before seeding the cells. Therefore, the majority of the reactive oxides were no longer on the surface of the samples when the cells attached. In addition, CaO may not have a damaging effect because it was most abundant on the HA sample, and after 7 days of culture, this sample had the highest number of cells among all the studied samples. Therefore, it does not seem reasonable to attribute the decrease in the proliferation rate to the presence of these oxides. Most likely, the dopant played an important role in proliferation. For example, if one excludes the possible negative effect attributed to CaO, the increase in the rate of cell proliferation observed for the Mn^{2+}-containing samples can be easily correlated with the presence of the Mn^{2+} ions in the samples.

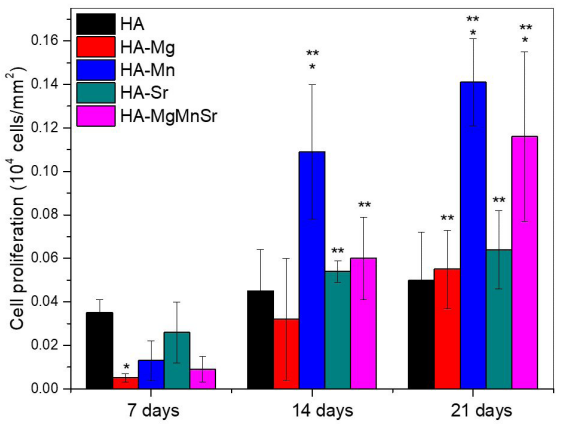

Figure 6. Typical time profile for MC3T3-E1 growth on the original and doped samples. *Significantly different from the HA sample at the same time point. **Significant difference between similar samples relative to the first time point (7 days).

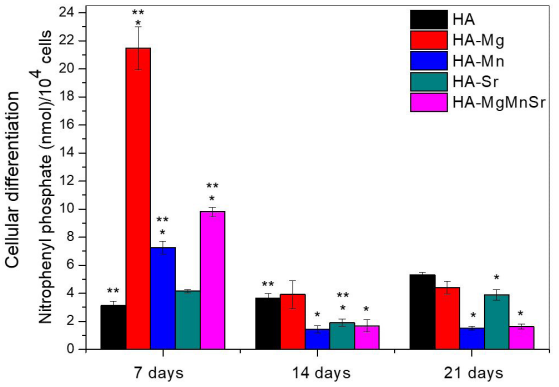

Figure 7. Cell differentiation of MC3T3-E1 on original and doped samples. *Significantly different from the HA sample at the same time point. **Significant difference between similar samples relative to the last time point (21 days).

The production of ALP by the cells reached its highest value after 7 days of culture for all samples (Figure 7). The behavior was the inverse of that observed for proliferation, which is in agreement with the literature. Preosteoblasts, such as MC3T3-E1 cells, differentiate into osteoblasts in a three-step process. The early stage (the proliferation phase) is characterized by substantial DNA synthesis and cell division, resulting in an increase in the cell number. The second stage (matrix maturation stage) is characterized by intense ALP expression, an early marker of osteoblastic differentiation. During the last phase (matrix mineralization), the cells demonstrate both ALP activity and mineralized nodules[50-53]. The ALP protein is secreted from the cells after synthesis, and its expression signals the phase at which differentiation is thought to be irreversible in most systems studied[54].

Herein, the presence of mature osteoblasts after the proliferation phase is indicated by the production of ALP. The exact mechanism by which this enzyme functions is not completely elucidated, but it seems to both increase the concentration of inorganic phosphates, a mineralization agent, and reduce the amount of extracellular pyrophosphates, an inhibitor of mineral formation[55]. The HA-Mg sample presented the highest level of ALP while exhibiting one of the lowest proliferation rates. Therefore, one can assume that Mg^{2+} stimulated differentiation faster than the other doping ions. In a previous report, Xue et al.[56] demonstrated that Mg^{2+}-doped calcium phosphate favors osteoblastic cellular attachment, proliferation, and ALP production. At the same time, the HA-Mn sample presented the highest proliferation rate and had a lower level of ALP relative to the Mg^{2+}-doped HA. One can conclude that Mn^{2+}-doped HA increases osteoblast differentiation more than nondoped HA but less than Mg^{2+}-doped HA. This indicates that although the Mn^{2+} ions accelerated cell growth, they also improved ALP production (osteoblast differentiation) compared to nondoped HA.

It is also important to note that the increase in cell proliferation promoted by the Mn^{2+} ions in HA-Mn was maintained in the multisubstituted HA sample (HA-MgMnSr). Most likely, the presence of Mn_3O_4 in both samples resulted in these similar effects. However, the differentiation increase induced by the presence of MgO in the HA-Mg sample was remarkably weaker in the HA-MgMnSr sample. Note that in this last sample, all the Mg^{2+} ions are preferentially included in the HA lattice and are not in the form of MgO. This indicates that the effect of Mg^{2+} on differentiation is quite dependent on the phase in which the Mg^{2+} ions are present, most likely because of the differences in solubility and, therefore, the release of the ions into the culture medium.

Considering both proliferation and differentiation assays, all the doped HA samples presented satisfactory results compared to the nondoped HA samples. The Mn^{2+} ions stand out since their incorporation into the apatite was more efficient and led to an outstanding proliferation rate at 21 days and an early differentiation peak at 7 days, indicating that mature osteoblasts were proliferating. Nevertheless, Mg^{2+} ions, which cause the opposite cell behavior, deserve special attention. However, it is clear that the Mg^{2+} ions were not inserted into the apatite lattice.

4. Conclusions

Mg^{2+} ions can stimulate cell differentiation, especially when segregated from the apatite structure in the form of MgO. However, the presence of MgO appears to considerably retard cell proliferation. At the same time, Mn^{2+} ions can increase cell proliferation and induce the production of high levels of ALP, regardless of whether the Mn^{2+} ions are inserted into the apatite structure or segregated in the form of Mn_3O_4. Finally, the presence of Sr^{2+} in the apatite lattice does not appear to directly affect cell behavior, since both proliferation and the production of ALP are comparable to those observed for the nondoped HA sample.

5. Acknowledgments

The authors acknowledge financial support from the Brazilian research agencies CNPq, FAPITEC/SE and CAPES in the form of the grant PROMOB CAPES/FAPITEC-SE (Nº 88881.157913/2017-01).

6. References

1. Szcześ A, Hołysz L, Chibowski E. Synthesis of hydroxyapatite for biomedical applications. Adv Colloid Interface Sci. 2017;249(April):321-30. http://dx.doi.org/10.1016/j.cis.2017.04.007. PMid:28457501.
2. O'Neill E, Awale G, Daneshmandi L, Umerah O, Lo KW-H. The roles of ions on bone regeneration. Drug Discov Today. 2018;23(4):879-90. http://dx.doi.org/10.1016/j.drudis.2018.01.049. PMid:29407177.
3. Robles-Águila MJJ, Reyes-Avendaño JAA, Mendoza MEE. Structural analysis of metal-doped (Mn, Fe, Co, Ni, Cu, Zn) calcium hydroxyapatite synthetized by a sol-gel microwave-assisted method. Ceram Int. 2017;43(15):12705-9. http://dx.doi.org/10.1016/j.ceramint.2017.06.154.
4. Robinson L, Salma-Ancane K, Stipniece L, Meenan BJ, Boyd AR. The deposition of strontium and zinc Co-substituted hydroxyapatite coatings. J Mater Sci Mater Med. 2017;28(3):51. http://dx.doi.org/10.1007/s10856-017-5846-2. PMid:28197823.
5. Šupová M. Substituted hydroxyapatites for biomedical applications: a review. Ceram Int. 2015;41(8):9203-31. http://dx.doi.org/10.1016/j.ceramint.2015.03.316.

6. Hughes JM, Rakovan JF. Structurally robust, chemically diverse: apatite and apatite supergroup minerals. Elements. 2015;11(3):165-70. http://dx.doi.org/10.2113/gselements.11.3.165.
7. Fihri A, Len C, Varma RS, Solhy A. Hydroxyapatite: a review of syntheses, structure and applications in heterogeneous catalysis. Coord Chem Rev. 2017;347:48-76. http://dx.doi.org/10.1016/j.ccr.2017.06.009.
8. Gruselle M. Apatites: a new family of catalysts in organic synthesis. J Organomet Chem. 2015;793:93-101. http://dx.doi.org/10.1016/j.jorganchem.2015.01.018.
9. Guidry MW, Mackenzie FT. Experimental study of igneous and sedimentary apatite dissolution. Geochim Cosmochim Acta. 2003;67(16):2949-63. http://dx.doi.org/10.1016/S0016-7037(03)00265-5.
10. Krneta S, Ciobanu CL, Cook NJ, Ehrig K, Kontonikas-Charos A. Apatite at Olympic Dam, South Australia: a petrogenetic tool. Lithos. 2016;262:470-85. http://dx.doi.org/10.1016/j.lithos.2016.07.033.
11. Troesch S, Esser D, Molle P. Natural rock phosphate: a sustainable solution for phosphorous removal from wastewater. Procedia Eng. 2016;138:119-26. http://dx.doi.org/10.1016/j.proeng.2016.02.069.
12. Gómez-Morales J, Iafisco M, Delgado-López JM, Sarda S, Drouet C. Progress on the preparation of nanocrystalline apatites and surface characterization: overview of fundamental and applied aspects. Prog Cryst Growth Charact Mater. 2013;59(1):1-46. http://dx.doi.org/10.1016/j.pcrysgrow.2012.11.001.
13. Elliott JC. Structure and chemistry of the apatites and other calcium orthophosphates. London: Elsevier; 1994.
14. Elliott JC. Calcium phosphate biominerals. Rev Mineral Geochem. 2002;48(1):427-53. http://dx.doi.org/10.2138/rmg.2002.48.11.
15. Andrés NC, D'Elía NL, Ruso JM, Campelo AE, Massheimer VL, Messina PV. Manipulation of Mg^{2+}-Ca^{2+} switch on the development of bone mimetic hydroxyapatite. ACS Appl Mater Interfaces. 2017;9(18):15698-710. http://dx.doi.org/10.1021/acsami.7b02241. PMid:28426935.
16. Nabiyouni M, Brückner T, Zhou H, Gbureck U, Bhaduri SB. Magnesium-based bioceramics in orthopedic applications. Acta Biomater. 2018;66:23-43. http://dx.doi.org/10.1016/j.actbio.2017.11.033. PMid:29197578.
17. Zilm ME, Yu L, Hines WA, Wei M. Magnetic properties and cytocompatibility of transition-metal-incorporated hydroxyapatite. Mater Sci Eng C. 2018;87(87):112-9. http://dx.doi.org/10.1016/j.msec.2018.02.018. PMid:29549940.
18. Anwar A, Akbar S. Novel continuous microwave assisted flow synthesis of nanosized manganese substituted hydroxyapatite. Ceram Int. 2018;44(9):10878-82. http://dx.doi.org/10.1016/j.ceramint.2018.03.141.
19. Frasnelli M, Cristofaro F, Sglavo VM, Dirè S, Callone E, Ceccato R, et al. Synthesis and characterization of strontium-substituted hydroxyapatite nanoparticles for bone regeneration. Mater Sci Eng C. 2017;71:653-62. http://dx.doi.org/10.1016/j.msec.2016.10.047. PMid:27987756.
20. Taha A, Akram M, Jawad Z, Alshemary AZ, Hussain R. Strontium doped injectable bone cement for potential drug delivery applications. Mater Sci Eng C. 2017;80:93-101. http://dx.doi.org/10.1016/j.msec.2017.05.117. PMid:28866230.
21. Quade M, Schumacher M, Bernhardt A, Lode A, Kampschulte M, Voß A, et al. Strontium-modification of porous scaffolds from mineralized collagen for potential use in bone defect therapy. Mater Sci Eng C. 2018;84:159-67. http://dx.doi.org/10.1016/j.msec.2017.11.038. PMid:29519425.
22. Bang LTT, Ramesh S, Purbolaksono J, Ching YCC, Long BDD, Chandran H, et al. Effects of silicate and carbonate substitution on the properties of hydroxyapatite prepared by aqueous co-precipitation method. Mater Des. 2015;87:788-96. http://dx.doi.org/10.1016/j.matdes.2015.08.069.
23. Alshemary AZ, Akram M, Goh Y-F, Tariq U, Butt FK, Abdolahi A, et al. Synthesis, characterization, in vitro bioactivity and antimicrobial activity of magnesium and nickel doped silicate hydroxyapatite. Ceram Int. 2015;41(9):11886-98. http://dx.doi.org/10.1016/j.ceramint.2015.06.003.
24. Wei L, Pang D, He L, Deng C. Crystal structure analysis of selenium-doped hydroxyapatite samples and their thermal stability. Ceram Int. 2017;43(18):16141-8. http://dx.doi.org/10.1016/j.ceramint.2017.08.189.
25. İnce T, Kaygili O, Tatar C, Bulut N, Koytepe S, Ates T. The effects of Ni-addition on the crystal structure, thermal properties and morphology of Mg-based hydroxyapatites synthesized by a wet chemical method. Ceram Int. 2018;44(12):14036-43. http://dx.doi.org/10.1016/j.ceramint.2018.04.257.
26. Silva LM, Menezes DS, Narayanan S, Shokuhfar T, Shahbazian-Yassar R, Dalmônico GML, et al. Counterions present in syntheses induce the precipitation of two different populations of Sr-containing hydroxyapatite crystals. Ceram Int. 2020;46(4):4502-10. http://dx.doi.org/10.1016/j.ceramint.2019.10.177.
27. Silva LM, Menezes DS, Almeida LE, Anselme K, Dentzer J, Santos EA, et al. The role of the counter-ions present in syntheses on the thermal stabilization of strontium and/or calcium apatites. Mater Sci Eng B. 2015;199:77-86. http://dx.doi.org/10.1016/j.mseb.2015.05.003.
28. Webler GD, Correia ACC, Barreto E, Fonseca EJS. Mg-doped biphasic calcium phosphate by a solid state reaction route: characterization and evaluation of cytotoxicity. Mater Chem Phys. 2015;162:177-81. http://dx.doi.org/10.1016/j.matchemphys.2015.05.055.
29. Bhattacharjee P, Begam H, Chanda A, Nandi SK. Animal trial on zinc doped hydroxyapatite: a case study. Journal of Asian Ceramic Societies. 2014;2(1):44-51. http://dx.doi.org/10.1016/j.jascer.2014.01.005.
30. Ullah I, Gloria A, Zhang W, Ullah MW, Wu B, Li W, et al. Synthesis and characterization of sintered Sr/Fe-modified hydroxyapatite bioceramics for bone tissue engineering applications. ACS Biomater Sci Eng. 2020;6(1):375-88. http://dx.doi.org/10.1021/acsbiomaterials.9b01666.
31. Moreira MP, de Almeida Soares GD, Dentzer J, Anselme K, de Sena LÁ, Kuznetsov A, et al. Synthesis of magnesium- and manganese-doped hydroxyapatite structures assisted by the simultaneous incorporation of strontium. Mater Sci Eng C. 2016;61:736-43. http://dx.doi.org/10.1016/j.msec.2016.01.004. PMid:26838904.
32. Silva LM, Menezes DS, Almeida LE, Anselme K, Dentzer J, Santos EA. The role of the counter-ions present in syntheses on the thermal stabilization of strontium and/or calcium apatites. Mater Sci Eng B Solid State Mater Adv Technol. 2015;199:77-86. http://dx.doi.org/10.1016/j.mseb.2015.05.003.
33. Marcus Y. Thermodynamics of solvation of ions. Part 5: gibbs free energy of hydration at 298.15 K. J Chem Soc, Faraday Trans. 1991;87(18):2995-9. http://dx.doi.org/10.1039/FT9918702995.
34. Santos EA, Pagano RL, Simoni JA, Airoldi C, Cestari AR, Vieira EFS. The influence of the counter ion competition and nature of solvent on the adsorption of mercury halides on SH-modified silica gel. Colloids Surf A Physicochem Eng Asp. 2002;201(1-3):275-82. http://dx.doi.org/10.1016/S0927-7757(01)01038-X.
35. Marques PA, Magalhães MC, Correia RN. Inorganic plasma with physiological CO_2/HCO_3- buffer. Biomaterials. 2003;24(9):1541-8. http://dx.doi.org/10.1016/S0142-9612(02)00539-2. PMid:12559814.
36. Shi J, Klocke A, Zhang M, Bismayer U. Thermallly-induced structural modification of dental enamel apatite: decomposition and transformation of carbonate groups. Eur J Mineral. 2005;17(5):769-76. http://dx.doi.org/10.1127/0935-1221/2005/0017-0769.
37. Santos SC, Lazaro GS, Santos EA. Ordering in sol-gel-derived bioactive glasses and its influence on the dissolution/precipitation

behavior in a complex culture medium. J Non-Cryst Solids. 2018;494:50. http://dx.doi.org/10.1016/j.jnoncrysol.2018.04.054.
38. Kumar GS, Thamizhavel A, Yokogawa Y, Kalkura SN, Girija EK. Synthesis, characterization and in vitro studies of zinc and carbonate co-substituted nano-hydroxyapatite for biomedical applications. Mater Chem Phys. 2012;134(2-3):1127-35. http://dx.doi.org/10.1016/j.matchemphys.2012.04.005.
39. Mostafa NY, Hassan HM, Abd Elkader OH. Preparation and characterization of Na+, SiO44-, and CO32-Co-substituted hydroxyapatite. J Am Ceram Soc. 2011;94(5):1584-90. http://dx.doi.org/10.1111/j.1551-2916.2010.04282.x.
40. Dorozhkin SV. Calcium orthophosphates in nature, biology and medicine. Materials. 2009;2(2):399-498. http://dx.doi.org/10.3390/ma2020399.
41. Fleet ME. Infrared spectra of carbonate apatites?? 2-Region bands. Biomaterials. 2009;30(8):1473-81. http://dx.doi.org/10.1016/j.biomaterials.2008.12.007. PMid:19111895.
42. Silvester L, Lamonier J-F, Vannier R-N, Lamonier C, Capron M, Mamede A-S, et al. Structural, textural and acid-base properties of carbonate-containing hydroxyapatites. J Mater Chem A Mater Energy Sustain. 2014;2(29):11073-90. http://dx.doi.org/10.1039/C4TA01628A.
43. El Feki H, Khattech I, Jemal M, Rey C. Thermal decomposition of carbonated containing sodium ions. Thermochim Acta. 1994;237(1):99-110. http://dx.doi.org/10.1016/0040-6031(94)85188-3.
44. Xu Y, An L, Chen L, Xu H, Zeng D, Wang G. Controlled hydrothermal synthesis of strontium-substituted hydroxyapatite nanorods and their application as a drug carrier for proteins. Adv Powder Technol. 2018;29(4):1042-8. http://dx.doi.org/10.1016/j.apt.2018.01.008.
45. Lüthen F, Bulnheim U, Müller PD, Rychly J, Jesswein H, Nebe JGGB. Influence of manganese ions on cellular behavior of human osteoblasts in vitro. Biomol Eng. 2007;24(5):531-6. http://dx.doi.org/10.1016/j.bioeng.2007.08.003. PMid:17884722.
46. Bose S, Fielding G, Tarafder S, Bandyopadhyay A. Understanding of dopant-induced osteogenesis and angiogenesis in calcium phosphate ceramics. Trends Biotechnol. 2013;31(10):594-605. http://dx.doi.org/10.1016/j.tibtech.2013.06.005. PMid:24012308.
47. Huang Y, Ding Q, Han S, Yan Y, Pang X. Characterisation, corrosion resistance and in vitro bioactivity of manganese-doped hydroxyapatite films electrodeposited on titanium. J Mater Sci Mater Med. 2013;24(8):1853-64. http://dx.doi.org/10.1007/s10856-013-4955-9. PMid:23686354.
48. Bose S, Tarafder S, Banerjee SS, Davies NM, Bandyopadhyay A. Understanding in vivo response and mechanical property variation in MgO, SrO and SiO2 doped β-TCP. Bone. 2011;48(6):1282-90. http://dx.doi.org/10.1016/j.bone.2011.03.685. PMid:21419884.
49. Roy M, Fielding GA, Bandyopadhyay A, Bose S. Effects of zinc and strontium substitution in tricalcium phosphate on osteoclast differentiation and resorption. Biomater Sci. 2013;1(1):74-82. http://dx.doi.org/10.1039/C2BM00012A. PMid:24244866.
50. Cicuéndez M, Silva VS, Hortigüela MJ, Matesanz MC, Vila M, Portolés MT. MC3T3-E1 pre-osteoblast response and differentiation after graphene oxide nanosheet uptake. Colloids Surf B Biointerfaces. 2017;158:33-40. http://dx.doi.org/10.1016/j.colsurfb.2017.06.019. PMid:28662392.
51. Koeneman KS, Yeung F, Chung LW. Osteomimetic properties of prostate cancer cells: a hypothesis supporting the predilection of prostate cancer metastasis and growth in the bone environment. Prostate. 1999;39(4):246-61. http://dx.doi.org/10.1002/(SICI)1097-0045(19990601)39:4<246::AID-PROS5>3.0.CO;2-U. PMid:10344214.
52. Magnusson P, Larsson L, Magnusson M, Davie MWJ, Sharp CA. Isoforms of bone alkaline phosphatase: characterization and origin in human trabecular and cortical bone. J Bone Miner Res. 1999;14(11):1926-33. http://dx.doi.org/10.1359/jbmr.1999.14.11.1926. PMid:10571693.
53. Peterson WJ. A method to assess the proliferative activity of small numbers of murine peripheral blood mononuclear cells. J Immunol Methods. 1987;96(2):171-7. http://dx.doi.org/10.1016/0022-1759(87)90311-5. PMid:3492561.
54. Seo H-J, Cho Y-E, Kim T, Shin H-I, Kwun I-S. Zinc may increase bone formation through stimulating cell proliferation, alkaline phosphatase activity and collagen synthesis in osteoblastic MC3T3-E1 cells. Nutr Res Pract. 2010;4(5):356-61. http://dx.doi.org/10.4162/nrp.2010.4.5.356. PMid:21103080.
55. Golub EE, Boesze-Battaglia K. The role of alkaline phosphatase in mineralization. Curr Opin Orthop. 2007;18(5):444-8. http://dx.doi.org/10.1097/BCO.0b013e3282630851.
56. Xue W, Dahlquist K, Banerjee A, Bandyopadhyay A, Bose S. Synthesis and characterization of tricalcium phosphate with Zn and Mg based dopants. J Mater Sci Mater Med. 2008;19(7):2669-77. http://dx.doi.org/10.1007/s10856-008-3395-4. PMid:18270806.